mater.scichina.com link.springer.com Published online 18 January 2023 | https://doi.org/10.1007/s40843-022-2315-9

Engineering charge-transfer interactions for red-emitting SrLa(Sc,Ga)O_4:Ce^{3+} phosphor with improved thermal stability

Zhiyu Yang[1†], Yifei Zhao[1,2†], Jumpei Ueda[3], Maxim S. Molokeev[4,5,6], Mengmeng Shang[7] and Zhiguo Xia[1,8*]

ABSTRACT **Blue-light-excitable red-emitting phosphors with high thermal stability are essential for fabricating white light-emitting diodes (WLEDs). Herein, Ce^{3+}-doped $SrLaScO_4$ (SLO:Ce^{3+}) phosphor is discovered to have an abnormal red emission band centered at 640 nm when excited at 440 nm. Spectroscopy and structural analyses confirm that Ce^{3+} ions occupy the [LaO_8] polyhedrons competitively, generating a strong crystal field splitting and a large Stokes shift to produce a red emission. To further restrict the thermal quenching of SLO:Ce^{3+}, charge-transfer engineering is implemented by incorporating a large electronegative Ga^{3+} in the Sc^{3+} site, which can attract more charges from nearby coordinating groups to decrease the electronic occupation at the bottom of the conduction band and thereby enlarge the band gap. Sc/Ga substitution in SrLa(Sc,Ga)O_4:Ce^{3+} enhances the thermal stability by increasing the intensity ratio from 15% to 31% at 150°C compared with 20°C. This is attributed to the efficient suppression of the thermally stimulated ionization process. This study presents a general design principle for discovering novel Ce^{3+}-doped red phosphors with good thermal stability for WLED applications.**

Keywords: Ce^{3+}, thermal stability, band gap, broadband red luminescence

INTRODUCTION

Phosphor-converted white-light-emitting diodes (pc-WLEDs) have been regarded as next-generation solid-state lighting sources due to their long lifetime, compactness in size, energy-saving, and environmentally friendly nature [1,2]. In addition to the maturing green and yellow phosphors, the design and discovery of efficient, stable, and low-cost red-emitting phosphors would significantly improve device performance [3]. Therefore, numerous researchers have focused on developing new lanthanide (Ln)-doped red-emitting phosphors except for Mn^{4+}-doped fluoride red phosphors [4,5]. Ce^{3+} and Eu^{2+} are the most effective activators with prominent broadband excitation and emission among all available Ln ions due to their characteristic 5d→4f allowed transitions [6,7]. Generally, the photoluminescence (PL) properties of Ce^{3+}- and Eu^{2+}-doped phosphors are closely related to the portable lowest 5d energy level, which is influenced by the nephelauxetic effect, the crystal field on the splitting (CFS) of the energy of the 5d state and the Stokes shift [8,9]. In addition to red-emitting nitride phosphors such as $CaAlSiN_3$:Eu^{2+}, a strong CFS and large Stokes shift facilitate the generation of broadband red emission in Eu^{2+}-doped oxide-based phosphors [8]. However, achieving red emission for Ce^{3+} in oxide hosts is rather difficult.

The normal luminescence in Fig. 1a defines the conventional relationship between Eu^{2+} and Ce^{3+} luminescence in the same oxide host. Dorenbos and coworkers [10,11] concluded that although Ce^{3+} possesses stronger CFS energy, a larger centroid shift, and a larger Stokes shift than Eu^{2+}, Ce^{3+} still exhibits a shorter-wavelength emission (Fig. 1a) due to its intrinsically higher free energy potential (49,340 cm^{-1}) than Eu^{2+} (34,000 cm^{-1}) when occupying the same cation site (Model 1 in Fig. 1b). An abnormal emission phenomenon could be observed when the host matrix possesses disparate cation sites where Ce^{3+} and Eu^{2+} occupy different sites competitively (Model 2 in Fig. 1c). For instance, we have previously reported that Eu^{2+} in $SrLaScO_4$:Eu^{2+} (SLO:Eu^{2+}) phosphor occupies Sr^{2+} sites and emits red light at 620 nm when excited by blue light, with a Stokes shift of 170 nm and a full width at half maximum (FWHM) of 84 nm (Fig. 1d) [12]. Contrary to the rules above, Ce^{3+}-doped $SrLaScO_4$ (SLO:Ce^{3+}) exhibits an emission band with a peak wavelength of 650 nm, a Stokes shift of 210 nm, and an FWHM of 207 nm at 77 K. The mechanism is assigned to the competitive site occupation of Ce^{3+} ions into [LaO_8] polyhedrons rather than [SrO_8], as given in Fig. 1c, which would

[1] State Key Laboratory of Luminescent Materials and Devices, Guangdong Provincial Key Laboratory of Fiber Laser Materials and Applied Techniques, Guangdong Engineering Technology Research and Development Centre of Special Optical Fibre Materials and Devices, School of Materials Science and Engineering, South China University of Technology, Guangzhou 510641, China
[2] Department of Applied Physics, The Hong Kong Polytechnic University, Hong Kong 999077, China
[3] Graduate School of Advanced Science and Technology, Japan Advanced Institute of Science and Technology (JAIST), Nomi, Ishikawa 923–1292, Japan
[4] Laboratory of Crystal Physics, Kirensky Institute of Physics, Federal Research Center KSC SB RAS, Krasnoyarsk 660036, Russia
[5] Department of Engineering Physics and Radioelectronic, Siberian Federal University, Krasnoyarsk, 660041, Russia
[6] Research and Development Department, Kemerovo State University, Kemerovo 650000, Russia
[7] Key Laboratory for Liquid-Solid Structural Evolution and Processing of Materials (Ministry of Education), School of Materials Science and Engineering, Shandong University, Jinan 250061, China
[8] School of Physics and Optoelectronics, South China University of Technology, Guangzhou 510641, China
[†] These authors contributed equally to this work.
[*] Corresponding author (email: xiazg@scut.edu.cn)

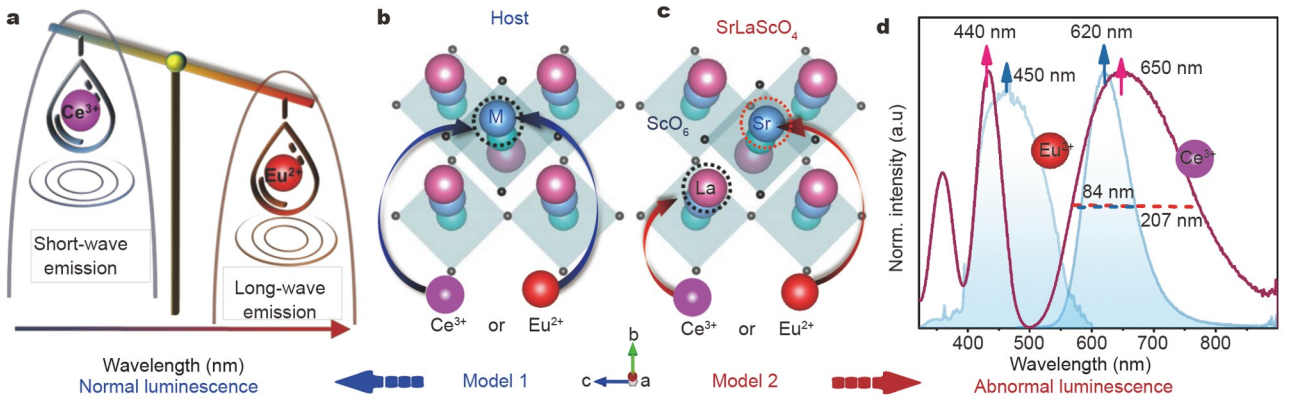

Figure 1 (a) Schematic diagram of the conventional relationship (normal luminescence) established by the Dorenbos's theory, where Ce^{3+} shows a shorter-wavelength emission than Eu^{2+} in the same local structure. (b) Schematic representation of the one host's crystal structure. Model 1 represents Ce^{3+} or Eu^{2+} entering the same cation sites, yielding a typical luminescence. (c) Crystal structure of SLO. Model 2 represents Ce^{3+} or Eu^{2+} entering different cation sites. (d) PL and PLE spectra of Ce^{3+} (pink curve) and Eu^{2+} (blue curve) in SLO; Ce^{3+} shows a longer-wavelength emission and broader FWHM than Eu^{2+} under 77 K due to Ce^{3+} or Eu^{2+} entering different cation sites (abnormal luminescence).

generate large Stokes shifts and CFS, leading to a longer-wavelength emission than that of SLO:Eu^{2+}. However, the thermal quenching of Ce^{3+} occupying trivalent cationic sites may be a major concern. For example, red-emitting $BaCa_2Y_6O_{12}$:Ce^{3+}: Ce^{3+}, $Sr_3Sc_4O_9$:Ce^{3+}, and $SrLu_2O_4$:Ce^{3+} possess poor thermal stability [3,11,13].

In general, thermal stability is a crucial criterion for evaluating the potential of phosphors for WLED applications. In Ce^{3+}-doped phosphors, thermal quenching will occur due to the non-radiative 5d→4f cross relaxation *via* electron-phonon coupling, resulting in a significant decrease in luminescent efficiencies [8,14,15]. The thermal quenching models also incorporate thermal ionization *via* excitation energy migration among dopants to quenching sites or/and thermally activated photo-ionization (TAP) of an electron from the Ce^{3+} $5d_1$ level to the conduction band (CB) [8,14,16]. Therefore, thermal stability is closely associated with host band gaps. If the 5d excited state is close to the bottom of CB, luminescent center energy is typically quenched by the TAP process [14]. Significant efforts have been made to increase the band gap of hosts by modifying their chemical compositions [17,18]. Combining density functional theory (DFT), Lin's group [19] recently proposed a charge-transfer engineering strategy by the rational regulation of the external coordination environment, where the resultant increase in band gap value was elucidated in detail. Increasing the band gap makes it possible to improve the thermal stability of activators in inorganic hosts.

Herein, the charge-transfer engineering was employed in SrLa(Sc,Ga)O_4:Ce^{3+} phosphor to effectively prevent the TAP process of Ce^{3+}, where Ga^{3+} with strong electronegativity was introduced to modify the chemical compositions and luminescence properties. Compared with the pure Sc in $SrLaScO_4$, Ga can attract more charges from nearby coordinated groups to decrease the electronic occupation at the bottom of the CB, resulting in a larger band gap. Under blue light excitation, $SrLaSc_{1-y}Ga_yO_4$:Ce^{3+} (abbreviated as SLG_yO:Ce^{3+}) exhibits the same emission and excitation band as SLO:Ce^{3+}. However, at room temperature (RT), an additional excitation band (300–380 nm) originating from the 4f→$5d_2$ transition appears. In addition, Ga^{3+} can help improve the thermal stability of SLO:Ce^{3+}, allowing emission intensities to be maintained between 15% and 31% higher at 150 than at 20°C. This is attributed to the reduced energy loss accompanied by the suppressed TAP process of Ce^{3+} $5d_1$ electrons to the CB. This research proposes a method for developing Ce^{3+}-doped red phosphors with improved thermal stability.

EXPERIMENTAL SECTION

Materials and synthesis

All chemicals, including $SrCO_3$ (99.9%, Aladdin), La_2O_3 (99.99%, Aladdin), Sc_2O_3 (99.99%, Aladdin), Ga_2O_3 (99.9%, Aladdin), and CeO_2 (99.99%, Aladdin) were used without further purification. The nominal SLO:$x$$Ce^{3+}$ (x = 0.01–0.20) and SLG_yO:0.08Ce^{3+} (y = 0.04–0.12) phosphors were synthesized using the high-temperature solid-state reaction method. According to the designed compositions, the stoichiometric concentrations of the raw materials were weighed and mixed. All the experimental steps were identical to those previously described for synthesizing SLO:Eu^{2+} [12].

Characterization

Powder X-ray diffraction (XRD) data were collected using an Aeris XRD diffractometer (PANalytical Corporation, Netherlands) operating at 40 kV and 15 mA with monochromatic Cu Kα radiation (λ = 1.5406 Å). The morphologies of phosphor particles were examined by an scanning electron microscope (SEM, NOVA NANOSEM 430), and the elemental mapping was characterized using the energy-dispersive X-ray spectroscopy (EDS) attached to the SEM. PL and PL excitation (PLE) spectra, and PL decay curves were measured using an Edinburgh Instruments FLS1000 equipped with both Xe and continuous (450 W) lamps. The samples' luminescence thermal quenching behavior was measured using the same spectrophotometer equipped with a high-temperature fluorescence instrument (Tian Jin Orient-KOJI Instrument Co., Ltd.). The low temperature-dependent spectra were measured with the same spectrophotometer fitted with a Cryo-77 low-temperature fluorescence device (Tian Jin Orient-KOJI Instrument Co., Ltd.). A Hitachi Corporation UH4150 ultraviolet-visible-near-infrared (UV-vis-NIR) spectrophotometer was used to acquire the diffuse reflection spectrum (DRS). X-ray photoelectron spectroscopy

(XPS, ESCALAB 250Xi) was used to determine the phosphor's surface element compositions and chemical change. The absolute quantum efficiency was measured by the absolute PL quantum yield spectrometer (Hamamatsu, C13534).

Computational method

To describe the exchange-correlation interactions within the material systems, DFT calculations were performed in the Vienna *ab initio* simulation package using the generalized gradient approximation with Perdew-Burke-Ernzerhof functional. In these calculations, the electronic configurations O ($2s^2 2p^4$), Sr ($4s^2 4p^6 5s^2$), Sc ($3p^6 3d^1 4s^2$), La ($5s^2 5p^6 5d^1 6s^2$), Ga ($4s^2 4p^1$), and Ce ($4f^1 5s^2 5p^6 5d^1 6s^2$) were considered. The plane-wave cutoff energy was set to 400 eV, and gamma-centered 3 × 3 × 3 *k*-meshes were utilized in the calculations. To satisfy the convergence criterion, the optimized structures' forces must not exceed 0.1 eV $Å^{-1}$, and their electronic energy must be less than 5.0×10^{-5} eV.

According to the experimental doping concentrations, the defect formation energies (E^f(defect)) for Ga- and Ce-doped SLO were calculated and compared based on different scales of supercells (approximately 3.1% Ce and 6.3% Ga, respectively). E^f(defect) was computed using the following Equation (1):

$$E^f(\text{defect}) = E_{\text{tot}}(\text{defect}) - E_{\text{tot}}(\text{pristine}) - \sum_i n_i \mu_i, \quad (1)$$

where E_{tot}(defect) and E_{tot}(pristine) are the total energies of the defective structure and the perfect structure, respectively. $\sum_i n_i \mu_i$ denotes the variation in chemical potentials following the introduction of defects. All the referencing chemical potentials μ_i are derived from the corresponding conventional phases, i.e., face center cubic (fcc) Ce, hexagonal close-packed (hcp) La, fcc Sr, hcp Sc, and orthorhombic Ga.

RESULTS AND DISCUSSION

Structure and site occupation

Fig. S1 and our previous report demonstrated a random distribution of Sr^{2+} and La^{3+} ions in SLO with a site occupancy ratio of 1:1 [12]. The phase purity of SLO:xCe^{3+} (x = 0.01, 0.08, and 0.20) samples was confirmed by powder XRD (Fig. 2a), and the Rietveld refinement analyses for all samples are illustrated in Fig. S2. All diffraction peaks are indexable on the standard SLO card (JCPDS No. 810857) [20]. In addition, all refinement results were stable and yielded low *R*-factors (Table S1). Tables S2 and S3 list the atomic coordinates and primary bond lengths. As seen in Fig. 2b, the decreased cell volumes of SLO:xCe^{3+} (x = 0.01–0.20) with increasing x(Ce) concentrations indicate that Ce^{3+} ions with smaller radii ($IR_{(Ce^{3+},CN=8)}$ = 1.14 Å) are inserted in Sr^{2+} and/or La^{3+} sites ($IR_{(Sr^{3+},CN=8)}$ = 1.26 Å), $IR_{(La^{3+},CN=8)}$ = 1.16 Å), leading to a lattice contraction (CN signifies the coordination number). Fig. 2c depicts an SEM image of a smooth particle of SLO:Ce^{3+} with sizes between 3 and 10 μm. In addition, elemental mapping images (Fig. 2d) demonstrate the uniform distribution of Sr, La, Sc, Ce, and O over the selected SLO:Ce^{3+} particle.

PL properties of SLO:Ce^{3+}

Upon excitation at 440 nm, SLO:Ce^{3+} emits an asymmetric broadband red light from 500 to 900 nm, centered at 640 nm (Fig. S3a). Comparatively, SLO:Eu^{2+} exhibits a peak red emission at 620 nm when Eu^{2+} occupies the Sr^{2+} site (Fig. 1d). At RT, the PLE spectrum of SLO:Ce^{3+} reveals one strong absorption peak (400–500 nm) and one nearly invisible absorption peak (330–380 nm). Since the optimal PL intensities are obtained at a Ce^{3+} concentration of 8%, this composition is used in the subsequent analyses. In general, two factors may contribute to the

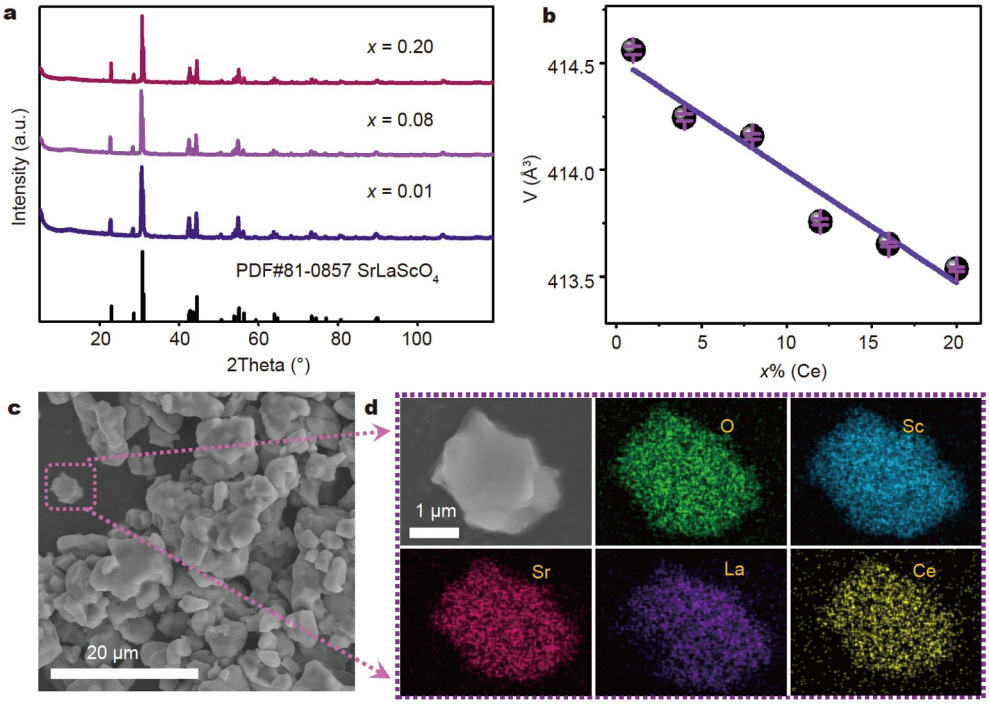

Figure 2 (a) XRD patterns of SLO:Ce^{3+} with different Ce^{3+} doping concentrations. (b) Dependence of the cell volume $V(x)$ per x(Ce) in the SLO:xCe^{3+} (x = 0.01–0.20). (c) SEM image of SLO:Ce^{3+} microcrystal particles. (d) Enlarged view of SLO:Ce^{3+} particle and the corresponding elemental mapping images of Sr, La, Sc, Ce, and O for the selected particle.

anomalous luminescent phenomenon in which Ce^{3+} shows a longer-wavelength emission than Eu^{2+} in the same host: the enormous Stokes shift and the unusually low-lying lowest 5d level [21]. The Stokes shift of SLO:Ce^{3+} is estimated to be 210 nm (7342 cm^{-1}) due to a significant structure relaxation [22,23]. In our case, the Stokes shift exceeds nearly all previously reported Ce^{3+}-doped phosphors, allowing for the exceptionally red-shifted emission (as compared in Table S4).

At 77 K, SLO:Ce^{3+} emits less energy with a larger FWHM than that of SLO:Eu^{2+} (Fig. 1d). In addition to the original absorption peak at 440 nm, a 300–380 nm absorption band with enhanced strength was discovered. Two excitation peaks at 360 and 440 nm are attributed to transitions from the ground state of 4f ($^2F_{5/2}$ and $^2F_{7/2}$) to the excited states of $5d_2$ and $5d_1$ in Ce^{3+} (Fig. 3a) [24]. As the temperature rises, the excitation band with a maximum at 360 nm weakens until it disappears at 277 K. Moreover, the PL spectra measured at 360-nm excitation exhibit a more severe thermal quenching than those measured at 440 nm (Fig. S3b, c). Therefore, it can be inferred that the $5d_2$-excited state has a stronger TAP, which will be discussed in greater detail later [14,25].

At RT, the PL spectra of SLO:Ce^{3+} under different excitation wavelengths exhibit identical emission profiles, indicating a single Ce^{3+} luminescence center in SLO:Ce^{3+} (Fig. S3d). In addition, at 77 K, the broad emission band decomposes into two Gaussian peaks with maxima at 15,481 cm^{-1} ($5d_1 \rightarrow {}^2F_{5/2}$) and 13,370 cm^{-1} ($5d_1 \rightarrow {}^2F_{7/2}$) (Fig. 3b), respectively [26]. The energy difference between the two Gaussian peaks is 2111 cm^{-1}, which is close to the theoretical value for that of the Ce^{3+} $^2F_{7/2}$ and $^2F_{5/2}$ states (2000 cm^{-1}), confirming the presence of a single crystallographic site in this host [21]. The spectral redshift is caused by the different responses of the $5d_1 \rightarrow {}^2F_{5/2}$ and $5d_1 \rightarrow {}^2F_{7/2}$ transitions to excitation wavelengths (Fig. S3d). Despite varying temperatures and excitation wavelengths, the decay curves of SLO:Ce^{3+} remain a single exponential model when monitoring the 640-nm emission (Fig. 3c). This provides additional evidence that Ce^{3+} occupies only a single site in SLO. Combining the refinement results with similar ionic radii and valence, we lean toward the $Ce^{3+} \leftrightarrow La^{3+}$ substitution. As depicted in Fig. S4, we have previously demonstrated that Eu^{2+} prefers to occupy the Sr^{2+} site in SLO, whereas Eu^{3+} incorporates the competitive La^{3+} sites. Similar to the trivalent cation La^{3+}, the trivalent cation Ce^{3+} tends to occupy the La^{3+} site with matched charge states. In addition, DFT calculations further indicate that Ce^{3+} would rather occupy La^{3+} (1.1 eV) than Sr^{2+} (1.4 eV) (Table 1). According to the following equations, the calculated crystal field strength of Ce^{3+} occupying La^{3+} is 12,269.9 cm^{-1} [27,28],

$$\varepsilon_{CFS} = \beta_{poly}^{Q} R_{av}^{-2}, \quad (2)$$

where Q is 3 for Ce^{3+}. β_{poly}^{Q} is a constant (β_{poly}^{Q} = 1.36 × 10^5 eV Pm^5). R_{av} is defined as

$$R_{av} = \frac{1}{n}\sum_{i=1}^{CN}\left(R_i - 0.6(R_M - R_{Ln})\right), \quad (3)$$

where R_i denotes the individual bond lengths to the CN coordinating anions in the unrelaxed lattice. R_M denotes the cationic radius, and R_{Ln} denotes the lanthanide ionic radius. As a result, the abnormal luminescent phenomenon of SLO:Ce^{3+} was attributed to the Ce^{3+} occupying the La^{3+} sites with large Stokes shift and CFS.

PL properties of $SrLa(Sc,Ga)O_4:Ce^{3+}$

Through XRD analysis, the phase purity of $SLGyO:Ce^{3+}$ (y = 0–0.12) was confirmed (Fig. S5). Fig. S6 depicts the XPS spectra of SLO:Ce^{3+} and $SLG_{0.12}O:Ce^{3+}$. The SEM images and EDS of $SLG_{0.12}O:Ce^{3+}$ are also acquired. Under 440-nm excitation, $SLG_yO:Ce^{3+}$ (y > 0) samples exhibit the same PL characteristics as SLO:Ce^{3+} (Fig. 4a), indicating that Ga^{3+} doping does not affect the original luminescence characteristics. In addition, an extra shoulder peak appeared at 360 nm in the PLE spectra of $SLG_yO:Ce^{3+}$ (Fig. 4b). Ga^{3+} can restructure the $5d_2$ level of SLO:Ce^{3+}, as the shoulder peaks' intensities increase with increasing Ga^{3+} concentrations. Combining the peak shift and DFT calculations, it is concluded that the Ga^{3+} ions occupy only Sc^{3+} sites in SLO (Fig. S5, Table 1). For the PL emission, a small amount of Ga^{3+} doping can increase the luminescent intensity of SLO:Ce^{3+}, and the luminescence quenching phenomenon will occur at Ga^{3+} concentrations above 0.08. Therefore, 9%, 15%, and 8% are the absolute quantum efficiencies for SLO:Ce^{3+}, $SLG_{0.08}O:Ce^{3+}$, and $SLG_{0.12}O:Ce^{3+}$, respectively. However, the extra shoulder peak observed at 360 nm increases continuously with Ga^{3+} concentration. To reveal the properties of $SLG_yO:Ce^{3+}$, the sample with y = 0.12 was chosen as a model for further characterization.

At 77 K, the shoulder peak of $SLG_{0.12}O:Ce^{3+}$ was significantly amplified and became dominant in the PLE spectra (Fig. 4c)

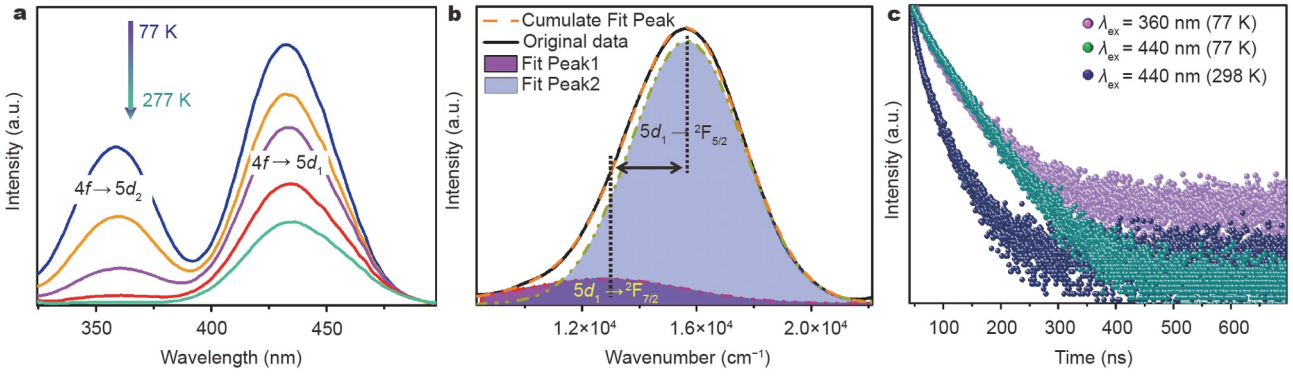

Figure 3 (a) PLE spectra of the typical SLO:Ce^{3+} sample from 77 to 277 K. (b) Gaussian fitting curves for the PL spectrum of SLO:Ce^{3+}. The broad emission band at 77 K can be decomposed into two Gaussian curves with maxima at 15,481 and 13,370 cm^{-1}, respectively. (c) Decay curves by monitoring the emission of Ce^{3+} at 640 nm under different excitation wavelengths and temperatures. At 77 K, the fitted decay lifetimes of Ce^{3+} in SLO:Ce^{3+} are 54.8 and 60.9 ns under 360- and 440-nm excitation, respectively. And the lifetime value is 32.5 ns under 298 K upon 440-nm excitation.

Table 1 Results of defect formation energy calculations based on different substitution models

Defect	Formula	E_{tot}(defect) (eV)	E^f(defect) (eV)
Ce_{La}	$Sr_{32}Sc_{32}CeLa_{31}O_{128}$	−1781.738	1.098209
Ce_{Sc}	$Sr_{32}Sc_{31}CeLa_{32}O_{128}$	−1777.148	1.143097
Ce_{Sr}	$Sr_{31}Sc_{32}CeLa_{32}O_{128}$	−1784.599	1.397386
Ga_{La}	$Sr_{16}Sc_{16}La_{15}GaO_{64}$	−882.8319	5.798793
Ga_{Sc}	$Sr_{16}Sc_{15}La_{16}GaO_{64}$	−882.6201	1.465964

while also exhibiting a higher absorption efficiency at RT (Fig. S7a, b). We inferred that substituting Sc/Ga could increase the transition probabilities of Ce^{3+} 4f→5d_2. Similar to SLO:Ce^{3+}, the PL spectra of $SLG_{0.12}O:Ce^{3+}$ exhibit a more severe thermal quenching of less than 360 nm excitation than those measured at 440 nm (Fig. S7c–e). To observe the transition line in the PLE spectrum, the energy level must be capable of receiving and storing the excitation energy required to produce luminescence. Suppose the signal from an energy level is absent from the PLE spectrum. In that case, this level is either incapable of absorbing excitation light or unable to store energy for further cross-correlation with the lowest excited states. Thus, the PL spectra can demonstrate radiative transitions, while the PLE spectra reveal non-radiative transitions between the 4f and 5d states [29]. Consequently, the lack of a high-energy band in the PLE spectrum (Fig. S3a) demonstrates the existence of strong non-radiative transitions for the Ce^{3+} 5d_2 level in SLO:Ce^{3+} under RT. The non-radiative transitions will be weakened at low temperatures, as evidenced by the newly formed excitation band with a maximum at 360 nm (Fig. 3a) and a longer decay lifetime value at low temperatures (54.8 ns, under 77 K) than at RT (32.5 ns, under 298 K) under 440-nm excitation (Fig. 3c). $SLG_{0.12}O:Ce^{3+}$ exhibits an observed absorption band (peaking at 360 nm) at RT, and the peak becomes dominant at 77 K, indicating that Ga^{3+}-doping can effectively suppress non-radiative transitions. At 77 K, the PL decay curve of $SLG_{0.12}O:Ce^{3+}$ exhibits a single exponential feature with a lifetime value comparable to that of SLO:Ce^{3+} (Fig. S8a, Fig. 3c). Together with the similar PL (peaking at 640 nm in Fig. S8b) and PLE (peaking at 440 nm in Fig. 4b) profiles, it was hypothesized that the 4f→5d_1 transitions of SLO:Ce^{3+} and $SLG_{0.12}O:Ce^{3+}$ are identical, indicating that Ga^{3+} can lower the 5d_2 energy level without affecting the 5d_1 level [8,14]. Consequently, it can be hypothesized that Ga^{3+} may provide a significant enhancement to combat the thermal quenching of SLO:Ce^{3+}. Indeed, the integrated PL intensity of SLO:Ce^{3+} is 15% at 150°C compared with the value before heating (Fig. 4d), whereas the integrated PL intensity of $SLG_{0.12}O:Ce^{3+}$ is 31% at 150°C, demonstrating the enhanced thermal stability brought about by Ga^{3+} doping (Fig. S8c, d). Therefore, the improvement can be ascribed to a decrease in TAP due to an increasing CB profile [14,30].

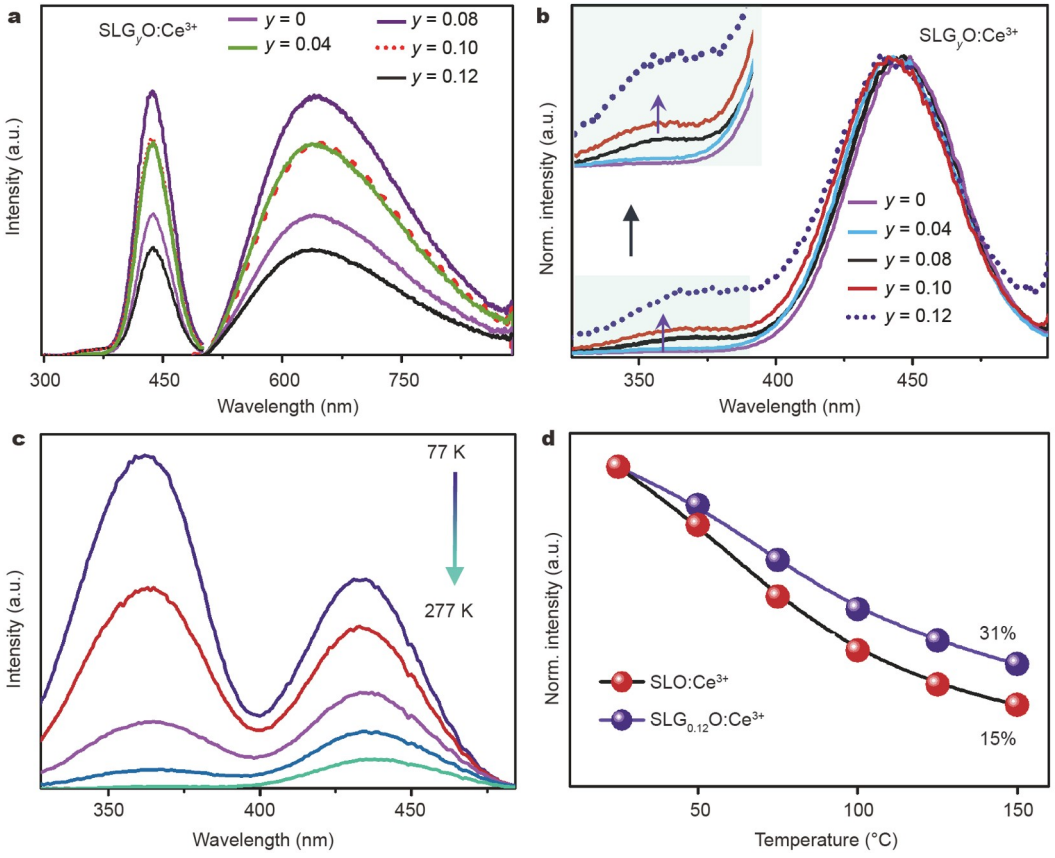

Figure 4 (a) PL and PLE spectra of SLG$_y$O:Ce^{3+} (y = 0–0.12) by monitoring at 440-nm excitation and 640-nm emission wavelengths. (b) Normalized PLE spectra of SLG$_y$O:Ce^{3+} (y = 0–0.12). The inset shows an enlarged view in the 330–390 nm range. (c) PLE spectra of $SLG_{0.12}O:Ce^{3+}$ by monitoring at 640 nm under low temperatures ranging from 77 to 277 K. (d) Normalized temperature-dependent integrated PL intensities of SLO:Ce^{3+} and $SLG_{0.12}O:Ce^{3+}$ monitored upon excitations less than 440 nm at various temperatures between 25 and 150°C.

Charge-transfer interaction visualization by DFT

DFT calculations were performed to investigate the Ga^{3+} dopant effect and to reveal the relationship between thermal stability and CB profile. First, the localized energy levels of Ce^{3+} (4f and 5d states) were determined in SLO. The density of states (DOS) diagram is depicted in Fig. 5a; the Ce 4f state is located in the middle of the bandgap, approximately 2 eV above the valance band of the host, whereas the 5d state lies at the bottom of CB. This energy level arrangement suggests that, despite SLO having a sufficient band gap to accommodate the localized Ce^{3+} levels, the energetically close distance between the 5d states and CB may significantly reduce the thermal stability *via* a potential TAP process. The electronegative Ga^{3+} is a potent tool for manipulating the host CB sites in relation to the localized Ce 5d states. As depicted in Fig. 5b–d, the newly formed Ga states (100-fold magnification) can effectively elevate the CB location, thereby increasing the gap between the localized Ce 5d state and the CB. The effect of Ga^{3+} is elucidated more clearly by the difference charge density diagrams (Fig. 5e). As depicted in Fig. 5f, g, the formation of the Ga–O bond will attract more electrons, reducing the covalency of other Sc–O bonds by reducing the accumulation of electrons [19]. Taking advantage of the negative correlation between covalency and the electronic band gap, it has been revealed that Ga^{3+} with a large electronegativity can effectively enlarge the band gap of SLO [19,31]. The band gap provides experimental confirmation of the concepts above. The E_g value from the DRS spectra was estimated using the following equation (Fig. 5h) [32]:

$$[F(R) \times h\nu]^2 = A(h\nu - E_g), \quad (4)$$

where $h\nu$ denotes the photon energy, A denotes the absorption constant, $F(R)$ denotes the absorption, and R denotes the reflectance coefficient (%). The calculated E_g increases from 2.83 and 2.90 to 2.94 eV with increasing Ga concentration. Theoretical and experimental results indicate that the SLO host can initially accommodate the Ce^{3+}-localized levels to facilitate the PL process. In addition, adding Ga to SLO can further elevate the CB to suppress the TAP process, thereby contributing to enhanced thermal stability.

Mechanism of restricted thermal quenching

Typically, the nephelauxetic effect will decrease the 5d levels of Ce^{3+} and Eu^{2+}, as determined by the bonding characteristics of the activator and ligands. Compared with Eu^{2+}, Ce^{3+} occupies the [LaO_8] polyhedron, resulting in a larger CFS. The vibrational rigidity of the host materials can increase the energy difference between the absorption and emission maxima. As depicted in the schematic energy level diagrams of Ce^{3+} and Eu^{2+} in the SLO host, these factors can reduce the energy separation between the 5d and 4f states, leading to abnormal long-wavelength emission (Fig. 6a). As stated previously, the TAP of electrons from the Ce^{3+} $5d_1$ level to the CB causes thermal quenching, which deteriorates with small band gaps, as depicted schematically in Fig. 6b for Ce^{3+} energy level diagrams, only the $4f \rightarrow 5d_1$ transitions of the Ce^{3+} ion can be observed in the PLE spectrum at RT. However, the extra $4f \rightarrow 5d_2$ transition can also be observed at

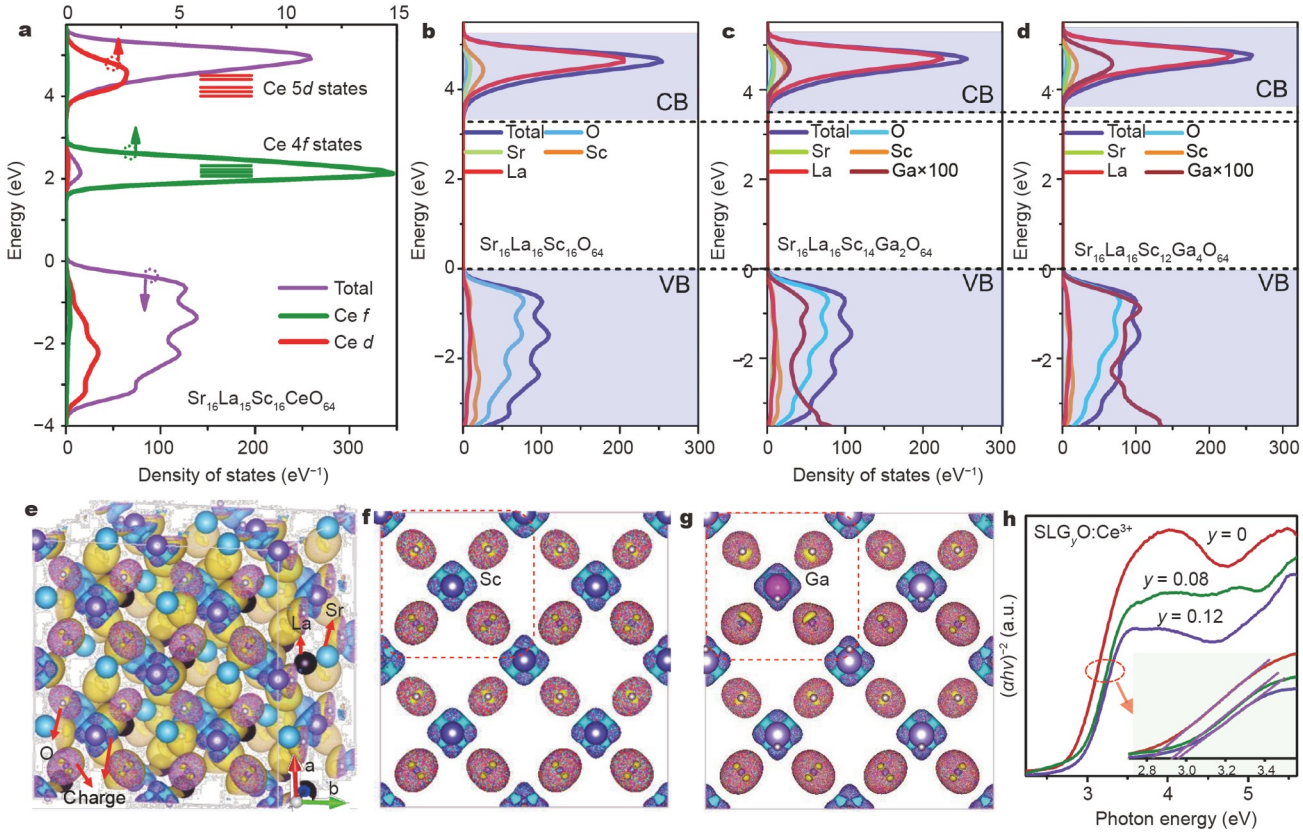

Figure 5 (a) Calculated DOS of SLO:Ce^{3+} featuring the projected DOS of Ce 4f and 5d states and the DOS of (b) SLO, (c) $SLG_{0.125}O$, and (d) $SLG_{0.25}O$. (e) Three-dimensional difference charge density diagram of SLGO and the two-dimensional difference charge density diagrams of (f) SLO and (g) SLGO of the corresponding (001) plane. (h) The fitted band gap values of $SLG_yO:Ce^{3+}$ according to the Tauc plot method.

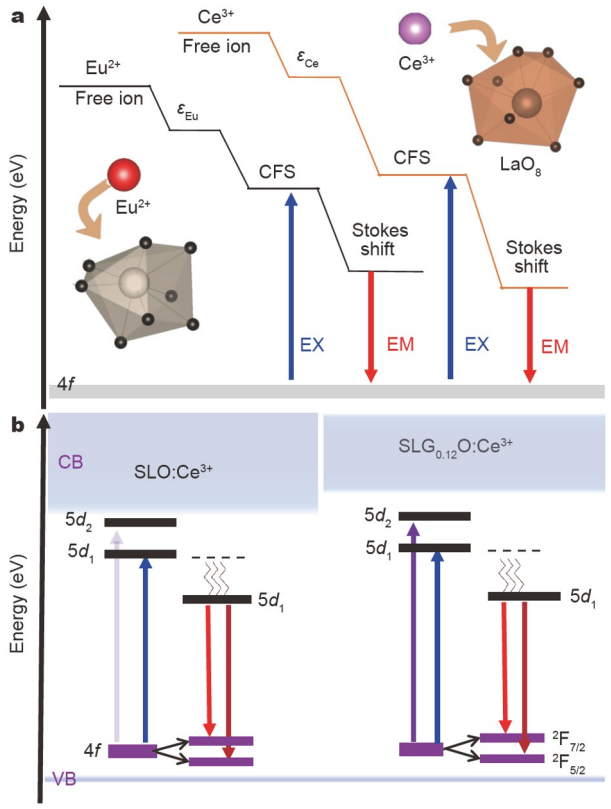

Figure 6 (a) Energy level diagrams of SLO:Ce^{3+} and SLO:Eu^{2+} where ε denotes the centroid shift of 5d states. The schematic depicts the incorporation of Ce^{3+} ions into the La^{3+} sites and Eu^{2+} ions into the Sr^{2+} sites. (b) Computed energy levels and the difference in Ce^{3+} ions in the SLO and SLGO *via* Sc/Ga substitution.

77 K, attributed to the suppressed TAP process at low temperatures. Taking advantage of the large band gap of $SLG_{0.12}O$, the Ce^{3+} $5d_2$-excited state separates from CB, contributing to a suppressed TAP even at high temperatures. Consequently, the $4f \rightarrow 5d_2$ transition is now observable at RT, and $SLG_{0.12}O:Ce^{3+}$ exhibits superior thermal quenching behavior compared with SLO:Ce^{3+}.

CONCLUSIONS

In conclusion, we have developed a novel broadband red-emitting SLO:Ce^{3+} phosphor with a peak emission wavelength of 640 nm when excited by blue light. SLO:Ce^{3+} exhibits a significantly longer-wavelength emission than SLO:Eu^{2+}, as demonstrated and elaborated. Herein, Ce^{3+} ions competitively enter the [LaO_8] polyhedron instead of [SrO_8], causing large Stokes and CFS to realize the lower energy emission. The stable substitution of Ga/Sc in SLO:Ce^{3+} generates an additional excitation band between 300 and 380 nm at RT and improves the thermal stability of SLO:Ce^{3+}. Experimental and theoretical evidence demonstrates that Ga^{3+} can increase the band gap in order to reduce the energy loss caused by the TAP of Ce^{3+} 5d electrons into the CB. This study provides significant guidance for the development of Ce^{3+}-doped red phosphors and a feasible strategy for the exploration of Ce^{3+}-doped oxide-based red phosphors with enhanced thermal stability.

Received 21 September 2022; accepted 4 November 2022; published online 18 January 2023

1 Zhao M, Zhang Q, Xia Z. Structural engineering of Eu^{2+}-doped silicates phosphors for LED applications. Acc Mater Res, 2020, 1: 137–145
2 Xia Z, Liu Q. Progress in discovery and structural design of color conversion phosphors for LEDs. Prog Mater Sci, 2016, 84: 59–117
3 Hasegawa T, Kim SW, Ueda T, *et al.* Unusual, broad red emission of novel Ce^{3+}-activated $Sr_3Sc_4O_9$ phosphors under visible-light excitation. J Mater Chem C, 2017, 5: 9472–9478
4 Xiao W, Liu X, Zhang J, *et al.* Realizing visible light excitation of Tb^{3+} *via* highly efficient energy transfer from Ce^{3+} for LED-based applications. Adv Opt Mater, 2019, 7: 1801677–1801683
5 Huang X. Homogeneous core-shell structure stabilizes Mn^{4+}-doped fluoride red phosphors for high-performance warm-white LEDs. Sci China Mater, 2019, 62: 1934–1935
6 Qiao J, Xia Z, Zhang Z, *et al.* Near UV-pumped yellow-emitting $Sr_9MgLi(PO_4)_7:Eu^{2+}$ phosphor for white-light LEDs. Sci China Mater, 2018, 61: 985–992
7 Huang X. High-throughput DFT screening enables the discovery of a super-broadband white-emitting phosphor for high-CRI white LEDs. Sci China Mater, 2020, 63: 325–326
8 Lin YC, Bettinelli M, Karlsson M. Unraveling the mechanisms of thermal quenching of luminescence in Ce^{3+}-doped garnet phosphors. Chem Mater, 2019, 31: 3851–3862
9 Hu T, Gao Y, Molokeev M, *et al.* Non-stoichiometry in $Ca_2Al_2SiO_7$ enabling mixed-valent europium toward ratiometric temperature sensing. Sci China Mater, 2019, 62: 1807–1814
10 Dorenbos P. Relation between Eu^{2+} and Ce^{3+} f ↔ d-transition energies in inorganic compounds. J Phys-Condens Matter, 2003, 15: 4797–4807
11 Hasegawa T, Iwaki M, Kim SW, *et al.* Blue-light-pumped wide-band red emission in a new Ce^{3+}-activated oxide phosphor, $BaCa_2Y_6O_{12}:Ce^{3+}$: Melt synthesis and photoluminescence study based on crystallographic analyses. J Alloys Compd, 2019, 797: 1181–1189
12 Yang Z, Liu G, Zhao Y, *et al.* Competitive site occupation toward improved quantum efficiency of $SrLaScO_4$:Eu red phosphors for warm white LEDs. Adv Opt Mater, 2022, 10: 2102373–2102381
13 Zhang S, Hao Z, Zhang L, *et al.* Observation of a red Ce^{3+} center in $SrLu_2O_4:Ce^{3+}$ phosphor and its potential application in temperature sensing. Dalton Trans, 2019, 48: 5263–5270
14 Senden T, van Dijk-Moes RJA, Meijerink A. Quenching of the red Mn^{4+} luminescence in Mn^{4+}-doped fluoride LED phosphors. Light Sci Appl, 2018, 7: 1–3
15 Tolhurst TM, Braun C, Schnick W, *et al.* Comprehensive band gap and electronic structure investigations of the prominent phosphors $M_2Si_5N_8:Eu^{2+}$ (M = Ca, Sr, Ba) determined using soft X-ray spectroscopy and density functional theory. J Phys Chem C, 2021, 125: 25799–25806
16 Ueda J, Dorenbos P, Bos AJJ, *et al.* Insight into the thermal quenching mechanism for $Y_3Al_5O_{12}:Ce^{3+}$ through thermoluminescence excitation spectroscopy. J Phys Chem C, 2015, 119: 25003–25008
17 Qiao J, Zhou Y, Molokeev MS, *et al.* Narrow bandwidth luminescence in $Sr_2Li(Al,Ga)O_4:Eu^{2+}$ by selective site occupancy engineering for high definition displays. Laser Photonics Rev, 2021, 15: 2100392
18 Zhao M, Xia Z, Huang X, *et al.* Li substituent tuning of LED phosphors with enhanced efficiency, tunable photoluminescence, and improved thermal stability. Sci Adv, 2019, 5: eaav0363
19 Mei D, Cao W, Wang N, *et al.* Breaking through the "3.0 eV wall" of energy band gap in mid-infrared nonlinear optical rare earth chalcogenides by charge-transfer engineering. Mater Horiz, 2021, 8: 2330–2334
20 Patel R, Simon C, Weller MT. $LnSrScO_4$ (Ln = La, Ce, Pr, Nd and Sm) systems and structure correlations for A_2BO_4 (K_2NiF_4) structure types. J Solid State Chem, 2007, 180: 349–359
21 Blasse G, Bril A. A new phosphor for flying-spot cathode-ray tubes for color television: Yellow-emitting $Y_3Al_5O_{12}$-Ce^{3+}. Appl Phys Lett, 1967, 11: 53–55
22 Wang S, Song Z, Kong Y, *et al.* Relationship of Stokes shift with composition and structure in Ce^{3+}/Eu^{2+}-doped inorganic compounds. J Lumin, 2019, 212: 250–263
23 Uken DA, Sergi A. Quantum dynamics of a plasmonic metamolecule with a time-dependent driving. Theor Chem Acc, 2015, 134: 141–149

24 Yao Q, Hu P, Sun P, *et al.* YAG:Ce^{3+} transparent ceramic phosphors brighten the next-generation laser-driven lighting. Adv Mater, 2020, 32: 1907888–1907895
25 Dorenbos P. Thermal quenching of Eu^{2+} 5d–4f luminescence in inorganic compounds. J Phys-Condens Matter, 2005, 17: 8103–8111
26 Im WB, Fellows NN, DenBaars SP, *et al.* $LaSr_2AlO_5$, a versatile host compound for Ce^{3+}-based yellow phosphors: Structural tuning of optical properties and use in solid-state white lighting. Chem Mater, 2009, 21: 2957–2966
27 Dorenbos P. Ce^{3+} 5d-centroid shift and vacuum referred 4f-electron binding energies of all lanthanide impurities in 150 different compounds. J Lumin, 2013, 135: 93–104
28 Yang Z, Zhao Y, Zhou Y, *et al.* Giant red-shifted emission in $(Sr,Ba)Y_2O_4:Eu^{2+}$ phosphor toward broadband near-infrared luminescence. Adv Funct Mater, 2021, 32: 2103927
29 Binnemans K. Interpretation of europium(III) spectra. Coord Chem Rev, 2015, 295: 1–45
30 Dorenbos P. Anomalous luminescence of Eu^{2+} and Yb^{2+} in inorganic compounds. J Phys-Condens Matter, 2003, 15: 2645–2665
31 Duan RH, Liu PF, Lin H, *et al.* $Ba_6Li_2CdSn_4S_{16}$: Lithium substitution simultaneously enhances band gap and SHG intensity. J Mater Chem C, 2017, 5: 7067–7074
32 Tauc J, Grigorovici R, Vancu A. Optical properties and electronic structure of amorphous germanium. Phys Stat Sol (b), 1966, 15: 627–637

Acknowledgements This work was supported by the National Key Research and Development Program of China (2021YFE0105700), the National Natural Science Foundations of China (51972118), the Natural Science Foundation of Shandong Province (ZR2021ZD10 and ZR2018JL016), Guangzhou Science & Technology Project (202007020005), and the Local Innovative and Research Teams Project of Guangdong Pearl River Talents Program (2017BT01X137). This work was also funded by Russian Foundation for Basic Research (19-52-80003).

Author contributions Xia Z conceived and designed the research. Yang Z performed the experiments. Zhao Y conducted the DFT calculations. Yang Z wrote the paper with support from Zhao Y. All authors contributed to the result interpretation.

Conflict of interest The authors declare that they have no conflict of interest.

Supplementary information Supporting data are available in the online version of the paper.

Zhiyu Yang is currently pursuing her PhD degree at the South China University of Technology under the supervision of Prof. Zhiguo Xia. She obtained her Master's degree from Yunnan Minzu University in 2019. Her current research interest mainly focuses on inorganic luminescent materials for solid-state lighting.

Yifei Zhao is currently pursuing a PhD degree at Hong Kong Polytechnic University. He obtained his Bachelor's and Master's degrees from the South China University of Technology in 2019 and 2021, respectively. His current research interest mainly focuses on ferroelectric thin films and devices.

Zhiguo Xia is a professor at the South China University of Technology. He obtained his Bachelor's degree in 2002 and Master's degree in 2005 from Beijing Technology and Business University and received his PhD degree from Tsinghua University in 2008. His research interests include the discovery of new rare earth-doped solid-state materials and the new luminescent metal halide crystals and their luminescence properties.

利用电荷转移工程提高红色$SrLa(Sc,Ga)O_4:Ce^{3+}$荧光粉的热稳定性

杨至雨[1†], 赵逸飞[1,2†], Jumpei Ueda[3], Maxim S. Molokeev[4,5,6], 尚蒙蒙[7], 夏志国[1,8*]

摘要 可被蓝光激发的高热稳定性红色荧光粉是制作高性能白光二极管(WLED)的关键材料. 研究发现, Ce^{3+}掺杂的$SrLaScO_4$ (SLO:Ce^{3+})荧光粉在440 nm激发下呈现峰值为640 nm的反常宽带红光发射. 光谱学和结构分析证实Ce^{3+}离子在SLO中进入[LaO_8]多面体, 产生强的晶体场劈裂和较大的Stokes位移, 实现了比Eu^{2+}更低能量的红光发射. 我们还设计并揭示了一种电荷转移相互作用的策略: 在Sc^{3+}位置引入电负性较大的Ga^{3+}, Ga^{3+}可以吸引更多邻位配合基团的电荷, 以减少导带底部的电子占用而扩大带隙. Sc/Ga取代有效地抑制了热激活电离过程, 使$SrLa(Sc,Ga)O_4:Ce^{3+}$的热稳定性获得了显著提升, 即在150°C的发光强度比(相对于20°C)从15%提升至31%. 本研究为发现具有良好热稳定性的新型Ce^{3+}掺杂红色荧光粉提供了有效的设计原则.